Flow Characteristics Inside MHD Seawater Thrusters

Ezzat Doss*
Argonne National Laboratory, Argonne, Illinois 60439
and
Gabriel Roy†
Office of Naval Research, Arlington, Virginia 22217

A three-dimensional MHD fluid-flow computer model has been developed and applied to study the concept of MHD seawater propulsion. The effects of strong magnetic fields on the current and electrical fields inside the MHD duct and their interaction with the flowfields, particularly those in the boundary layers, have been investigated. Results of parametric studies for variables influencing the flowfield characteristics and the overall performance of the propulsion systems are discussed. Such parameters include the magnetic field and electrical loading of the MHD thruster. The results of the calculations performed indicate the sensitivity of the thruster performance to the load factor and wall friction. The nonuniform distribution of the current density in the Hartmann layers of the insulating sidewalls causes the flattening of the velocity profiles on the sidewalls relative to the velocity profiles over the electrode walls. These nonuniformities in the flowfield give rise to nonuniform distribution of the skin friction along the walls of the thrusters, where higher values are predicted over the sidewalls relative to those over the electrode walls. Although the discrepancies of the velocity profiles between the different walls of the MHD thruster are not significant, careful considerations should be given to the calculation of the frictional losses because of their adverse effect on the electrical efficiency of the thruster.

Nomenclature

B	=	magnetic field
C_1, C_2, C_μ	=	constants in the turbulence model
C_f	=	skin friction coefficient
D	=	duct diameter, or height
$\boldsymbol{E}$	=	electric field vector
E_x, E_y, E_z	=	components of $\boldsymbol{E}$
G	=	generation of turbulence energy
H	=	channel height (distance between electrode walls)
I	=	load current
J_x, J_y, J_z	=	current components in x, y, z directions
$\boldsymbol{J}$	=	current vector
K	=	load factor
k	=	turbulence kinetic energy
L	=	duct length
p	=	static pressure
Q	=	flow rate
u, v, w	=	components of velocity vector along x, y, and z directions
V	=	applied external voltage
x, y, z	=	coordinate directions
δ	=	boundary-layer thickness
ρ	=	fluid density
τ	=	shear stress
σ	=	electrical conductivity
σ_k, σ_ε	=	turbulent Prandtl members for k and ε
ε	=	dissipation rate of turbulence energy
μ_o	=	permeability of free space
μ_τ	=	turbulent viscosity
μ_l	=	laminar viscosity
ϕ	=	electrical potential
β	=	Hall parameter
η	=	electric efficiency

Subscripts

cl	=	centerline
e	=	electrical
sw	=	sidewall
W	=	wall

Received Dec. 4, 1989; revision received Sept. 5, 1990; accepted for publication Sept. 12, 1990. Copyright © 1990 by the American Institute of Aeronautics and Astronautics, Inc. All rights reserved.

*Section Manager, Engineering Physics Division. Member AIAA.
†Scientific Officer, Propulsion. Associate Fellow AIAA.

Introduction

THERE is considerable renewed interest in the possibility of using the magnetohydrodynamic (MHD) concept for propelling submersibles or surface ships. This idea has been examined in the past by several investigators[1–6] and was found to have sufficient merit to warrant further studies, provided the applied magnetic field is high.

MHD seawater propulsion offers several advantages over conventional mechanical propellers. For example, the absence of a mechanical propeller system will lead to a reduced vibration level in the ship or submarine, and, thus, to a reduction in the mechanical noise generated. Also, there is no physical restriction on the speed of potential MHD seawater vehicles, whereas the speed of conventional propellers is limited by cavitation. Therefore, there is a potential to operate submarines and ships at higher speeds. Quieter and faster ships or submarines are desirable for obvious reasons. MHD seawater propulsion has the potential to achieve these goals at reasonable propulsion efficiencies.

MHD seawater propulsion depends on the conductivity of the seawater to carry the electric currents. Energy is supplied to the duct of the thruster by applying an external electric field. The resulting electric current $\boldsymbol{J}$ interacts with the applied magnetic field B to produce a driving $(\boldsymbol{J} \times B)$ Lorentz force that pushes the seawater through the duct. The MHD thruster, therefore, can be viewed as an electromagnetic pump that ejects the seawater at a higher velocity than the intake velocity, thus providing the thrust. Figure 1 shows a schematic diagram of the concept of MHD seawater thruster.

In order to increase the propulsion efficiency, the MHD forces have to be large. This can be achieved basically by either increasing the fluid electrical conductivity or by increasing the magnetic field. One can enhance the conductivity of seawater by any seeding procedure. However, this has the drawback of leaving a detectable signature of high-conduc-

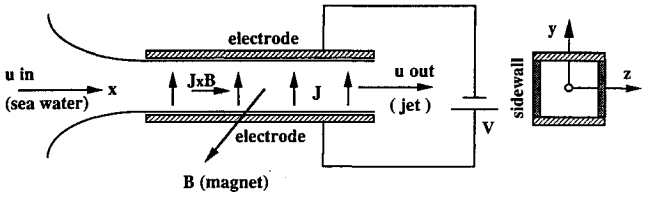

Fig. 1 A schematic diagram of the concept of MHD Thruster.

tivity fluid behind the surface ship or submarine, unless it be possible to recover the conducting fluid at the stern—an option not practical for continuous normal operation. This conclusion leaves the other option of increasing the magnetic field as an open possibility.

The effect of magnetic field strength on the propulsion efficiency has been studied by different researchers in the past, using simple physical relationships. For example, Phillips[1] carried out a feasibility study of MHD ship propulsion using different magnet configurations for propelling 600-ft. submarines. He found that the overall efficiency of the propulsion system of the submarine moving at a speed of 10 knots with a conventional iron-core magnet of 0.6 T is only 8%. His conclusion was that low efficiency and thrust would make the system unlikely to be useful as auxiliary propulsion unless a very large magnetic field is applied. To demonstrate the need for higher magnetic fields, Doragh[2] carried out an investigation in which he showed that a system propulsion efficiency of 60% could be achieved at a speed of 10 knots with a magnetic field of 10 T.

These studies, and also simple back-of-the-envelope calculations using basic physics laws, lead to one conclusion, i.e., a superconducting magnet with a high magnetic field must be used if one expects to achieve a practical MHD propulsion efficiency. Stewart Way of Westinghouse[3] carried out a pioneering experiment with a submarine model, 10-ft. long and 900-lb. displacement, to demonstrate the proof-of-concept of MHD propulsion. He has also performed a parametric study for submarine tankers having submerged displacements of 25,000, 50,000, and 100,000 tons. The corresponding computed propulsion efficiencies for a magnetic field of 7 T and cruise speed of 29 knots were 86, 83, and 79%, respectively. Similar results regarding the enhancement of propulsion efficiency have been discussed by Hummert[5] and Cott et al.[6]

Outside the U.S., Japan and the Soviet Union have shown interest in MHD propulsion. For example, Saji et al.[4] performed a parametric study for a 10,000 ton submarine tanker. They varied the magnetic field between 1 and 10 T and the submarine velocity between 10 and 60 knots. Their calculations agreed with Doragh's prediction of 60% efficiency with a magnetic field of 10 T. Also, their calculations indicated that the system propulsion efficiency drops significantly to less than 5% for a magnetic field strength of 1 T.

The operation of magnets using superconducting materials required cryogenic cooling with liquid helium, i.e., operation at 4.2 K. Also, sophisticated magnet designs operating in the 5–6 T range were not generally available on a large-scale production basis. Further, an extreme cryogenic environment, with its accompanying cumbersome refrigeration and containment system, was required; hence, MHD propulsion was judged to be infeasible at that time. However, recent developments in high-temperature superconducting materials have renewed international interest in reviving the concept of electromagnetic ship propulsion. The critical temperature for the new types of superconductors now extends to about 100 K, which is well above the 77 K boiling point of liquid nitrogen. Cryogenic cooling with liquid nitrogen is significantly simpler and cheaper than cooling with liquid helium, and nitrogen can be easily liquified and stored in ships or submarines.

This conclusion, namely, the need for superconducting magnets with high magnetic fields (10–20 T), opens the door for very important technical issues, among them how much can those high magnetic fields alter or modify the flowfields inside the MHD duct, and what are their effects on the thruster performance. In order to answer these questions, three-dimensional computer models are needed to solve for the electrical and current density fields in the cross section of the MHD ducts as an integral part of three-dimensional calculations of the flowfields. That is the purpose of this paper.

Comparison of Flow Parameters Between MHD Seawater Thrusters and Open-Cycle MHD Generators

Exhaustive work has been done on MHD channel flow for open-cycle plasma power generation, but the research effort on duct flow for seawater MHD propulsion is minimal. However, MHD flow inside ducts is subject to $J \times B$ forces whether the duct is an MHD generator or a thruster (accelerator). In the first case, electrical power is extracted from the interaction of the fluid flow with the magnetic field. In the second case, energy is supplied to the duct by applying an external electrical field. The resulting electrical currents interact with the magnetic field to produce a driving force that pushes the fluid through the duct. There are obviously some differences between the flow medium and the operating conditions between the two cases; however, the governing equations and the physical phenomena are quite similar.

In order to place the flow parameters for seawater propulsion in perspective, a comparison is made between the expected operating parameters for MHD propulsion and those for open-cycle MHD power generation. Table 1 lists these parameters. In turn, these physical parameters can be used to estimate several important dimensionless groups governing the flowfields inside MHD ducts and, hence, the MHD thrust efficiency. The dimensionless groups include the following:

1) Reynolds number—$R_n = \rho u D/\mu$
2) Magnetic Reynolds number—$(R_n)_m = \mu_o \sigma u L$
3) Hartmann number—$H_a = (\sigma B^2 D^2/\mu)^{1/2}$
4) Interaction parameters—$(I_u = \sigma B^2 L/u, I_p = \sigma u B^2 L/p)$

It can be seen from Table 1 that there are many similarities between the applications of MHD for open-cycle power generation and for seawater propulsion. The calculated values of the dimensionless parameters indicate that, in some cases when strong magnetic interaction with the flow occurs, the velocity fields may be distorted.

In MHD generators, the flowfields and electrical fields are inherently three-dimensional for a variety of reasons. The interaction of the MHD electrical forces ($J \times B$) with the

Table 1 Operating parameters for open-cycle power MHD generation and seawater propulsion

Parameter	OC-MHD	Seawater thruster
mode	generator	accelerator
(electric load factor)	<1.0	>1.0
working fluid	combustion gases	seawater
seed	potassium (or equivalent)	none
U, m/s	700–1100	10–40
T, K	2200–3000	300
Δp, atm	6–10	0.5–5
ρ, kg/m^3	~1	~10^3
L, m	8–15	10–30
D, m	0.5–2.0	1–3
B, Tesla	4–8	8–20
σ, S/m	4–10	4–5
β	0.3–4.0	0
electrode	segmented	continuous
$R_n(\rho UD/\mu)$	>10^7–10^8	~10^7–10^8
$(R_n)_m(\mu_o \sigma UL)$	<<1.0	<<1.0
$H_a(\sigma B^2 D^2/\mu)^{1/2}$	~10^3	~10^2–10^3
$I_p(\sigma U B^2 L/\Delta p)$	>1.0	~0.1–1.0
$I_u(\sigma B^2 L/\rho U)$	>1.0	~0.1–1.0

fluid flow leads to flow distortions.[7–9] The cross-sectional nonuniformity of the axial component of the Lorentz force ($J \times B$) is directly responsible for flattening the velocity profile along the insulating sidewalls, and for the possible generation of velocity overshoots in the boundary layers. The nonuniformity in the magnetic field direction of the Lorentz force, due to Hall current, produces secondary flows that in turn lead to flow asymmetry.

For MHD seawater thrusters, however, the electrical conductivity of seawater is expected to be practically uniform across and along the thruster, and the Hall parameter is negligible. Therefore, one might anticipate that such flow nonuniformities would not be manifested strongly inside the ducts, such as is the case of plasma generators. However, the calculation of the three-dimensional flow and electrical fields is warranted to investigate the extent of such flow nonuniformities inside the MHD thrusters.

MHD Three-Dimensional Thruster Model

A three-dimensional MHD generator model, which incorporates fully the interaction between the flowfields and the electrical fields inside the MHD duct,[8,9] has been adapted for the application of seawater propulsion. The flowfields are represented by the three-dimensional compressible turbulent Navier-Stokes equations, and their solution is coupled to the solution of the electric field in the crossflow direction. Since the flow is predominantly in the axial direction, the parabolic approximation is invoked in which the diffusional fluxes in the axial direction are neglected, and the pressure gradient in the axial momentum equation is considered uniform over the duct cross section. The parabolic approximation does not introduce any significant errors as long as the flow is predominantly unidirectional, but it makes the calculation procedure very economical from the computational viewpoint, particulary when one seeks a parametric evaluation of the concept of MHD propulsion.

The equations solved in this model consist of the mass conservation equation, the three momentum equations, and the Maxwell and Ohms law equations. The turbulent fluxes are computed using a two-equation model of turbulence in which partial differential equations are solved for the turbulence kinetic energy and its dissipation rate.

The following is a brief description of the main MHD flow equations and their method of solution.

Mean Flow Equations

$$\text{Mass continuity: } \frac{\partial}{\partial x}(\rho u) + \frac{\partial}{\partial y}(\rho v) + \frac{\partial}{\partial z}(\rho w) = 0 \tag{1}$$

$$X\text{-momentum: } \frac{\partial}{\partial x}(\rho uu) + \frac{\partial}{\partial y}(\rho vu) + \frac{\partial}{\partial z}(\rho wu) = -\frac{\partial p}{\partial x} + \frac{\partial \tau_{xy}}{\partial y} + \frac{\partial \tau_{xz}}{\partial z} + J_y B \tag{2}$$

$$Y\text{-momentum: } \frac{\partial}{\partial x}(\rho uv) + \frac{\partial}{\partial y}(\rho vv) + \frac{\partial}{\partial z}(\rho wv) = -\frac{\partial p}{\partial y} + \frac{\partial \tau_{yy}}{\partial y} + \frac{\partial \tau_{yz}}{\partial z} - J_x B \tag{3}$$

$$Z\text{-momentum: } \frac{\partial}{\partial x}(\rho uw) + \frac{\partial}{\partial y}(\rho vw) + \frac{\partial}{\partial z}(\rho ww) = -\frac{\partial p}{\partial z} + \frac{\partial \tau_{zy}}{\partial y} + \frac{\partial \tau_{zz}}{\partial z} \tag{4}$$

For seawater applications, ρ is assumed to be constant; its value depends on the physical location and temperature of the seawater.[10]

It has been found, in this application, that there is no need to solve for the temperature (or enthalpy) equation because of the negligible change of seawater temperature inside the duct, due to Joulean heating.

Turbulence Model

The turbulent fluxes are represented as the product of a turbulent viscosity and the gradients of the flow variable. The turbulent viscosity is calculated from the local values of the turbulent kinetic energy k and its dissipation rate ε, from the formula

$$\mu_t = C_\mu \rho k^2/\varepsilon \tag{5}$$

The turbulent fluxes are calculated by the following formulae:

$$\tau_{ij} = (\mu_t + \mu_l)\left(\frac{\partial u_i}{\partial x_j} + \frac{\partial u_j}{\partial x_i}\right) \tag{6}$$

The values of k and ε are obtained from the solution of the following transport equations:

$$\text{Kinetic energy of turbulence: } \frac{\partial}{\partial x}(\rho uk) + \frac{\partial}{\partial y}(\rho vk) + \frac{\partial}{\partial z}(\rho wk) = \frac{\partial}{\partial y}\left(\frac{\mu_t}{\sigma_k}\frac{\partial k}{\partial y}\right) + \frac{\partial}{\partial z}\left(\frac{\mu_t}{\sigma_k}\frac{\partial k}{\partial z}\right) + G - \rho\varepsilon \tag{7}$$

$$\text{Dissipation rate: } \frac{\partial}{\partial x}(\rho u\varepsilon) + \frac{\partial}{\partial y}(\rho v\varepsilon) + \frac{\partial}{\partial z}(\rho w\varepsilon) = \frac{\partial}{\partial y}\left(\frac{\mu_t}{\sigma_\varepsilon}\frac{\partial \varepsilon}{\partial y}\right) + \frac{\partial}{\partial z}\left(\frac{\mu_t}{\sigma_\varepsilon}\frac{\partial \varepsilon}{\partial z}\right) + \frac{C_1 G\varepsilon}{k} - C_2\rho\frac{\varepsilon^2}{k} \tag{8}$$

where G represents the production of the kinetic energy of turbulence as a result of the interaction of the shear stresses and the velocity gradients.

The expression for G, after neglecting the axial gradients, is as follows:

$$G = \mu_t\left\{2\left[\left(\frac{\partial v}{\partial y}\right)^2 + \left(\frac{\partial w}{\partial z}\right)^2\right] + \left(\frac{\partial u}{\partial y}\right)^2 + \left(\frac{\partial u}{\partial z}\right)^2 + \left(\frac{\partial v}{\partial z} + \frac{\partial w}{\partial y}\right)^2\right\} \tag{9}$$

Electrical Equations

Under the MHD approximations, the electric field $\boldsymbol{E}$ and the current density $\boldsymbol{J}$ are governed by the following Maxwell equations and Ohms law:

$$\text{Maxwell equations: } \nabla \times \boldsymbol{E} = 0, \qquad \nabla \cdot \boldsymbol{J} = 0 \tag{10}$$

$$\text{Ohms law: } \boldsymbol{J} = \sigma(\boldsymbol{E} + \vec{u} \times \boldsymbol{B}) \tag{11}$$

In the above, the magnetic field $\boldsymbol{B}$ is assumed uniform at each cross-sectional area of the duct, and is oriented along the z-direction. Also, in this application the Hall parameter β is taken to be zero, because it is negligible for seawater.

To simplify the solution procedure of the electrical equations, the electrical fields are assumed to vary slowly in the flow direction, in comparison to their variation in the crossflow direction. Such an assumption is reasonable along the bulk of an MHD duct away from the entrance and exit. In this formulation, an electrical potential $\phi\ (y, z)$ is defined, such that

$$\boldsymbol{E} = -\nabla \Phi \tag{12}$$

As a consequence of the assumed slow axial variation of the electric fields, E_x is constant at each cross section. By substituting Eq. (12) into Ohms Law [Eq. (11)], the following equation for the two-dimensional function for $\phi(y, z)$ results:

$$\frac{\partial}{\partial y}\left(\sigma\frac{\partial \Phi}{\partial y}\right) + \frac{\partial}{\partial z}\left(\sigma\frac{\partial \Phi}{\partial z}\right) = -\frac{\partial}{\partial y}(\sigma u B) \qquad (13)$$

An applied electric field, in terms of a load factor K, is specified as the boundary condition for the electrode walls; the sidewalls are assumed to be insulators.

Solution Procedure

The procedure used to solve the partial-differential equations employs a marching scheme, in which the solution to the differential equations is obtained at successive cross-sectional planes from the inlet to the exit of the duct. Because it was assumed that the flow is predominantly unidirectional, the influences always propagate along the flow direction and, therefore, the flow properties at a given axial station can be calculated solely from their values at the previous station. This eliminates the need to iterate back and forth between the inlet and the exit of the channel.

At each axial station, the equations for u, v, w, k, ε, and the electric potential are solved in their finite-difference form. The pressure fields are obtained from the satisfaction of the continuity equation. The details of the finite-differencing are given in Refs. 8 and 9. The finite-difference equations are solved by the tridiagonal matrix algorithm, and the convergence of the solution is rapid. One main consequence of the marching algorithm is that all the flow variables are stored only as two-dimensional arrays. This significantly reduces the required computer storage and CPU time.

The stability and accuracy of this numerical procedure have been established and discussed in detail in Ref. 9, evidenced by the good agreement achieved between the predictions of the computer model and the experimental data obtained from MHD generators. For the present applications, the accuracy of the predictions has been tested further by performing the computations for different axial step sizes and for different number of grid points across the duct.

Applications and Results

Operating Conditions

Computations have been performed using the three-dimensional model for MHD thruster operating in the continuous electrode mode with insulating sidewalls. The general operating parameters for the computational cases considered are listed in Table 2. The thruster is assumed 10 m long, with constant cross-sectional area of 1×1 m^2. The magnetic field is assumed to be constant along the duct. The flow at the entrance of the thruster is assumed to be that of a plug flow.

Table 2 Operating conditions for the illustrated examples

Thruster geometry:		
• length	10	m (rectangular)
• height and width	1×1	m^2
• wall roughness	2.5	mm
Wall temperature	300	K
Fluid temperature	300	K
Working fluid:	Seawater	
• electrical conductivity	4.8	S/m
• mass density	1025	Kg/m^3
• viscosity	$1.1\ 10^{-3}$	Kg/(m.s)
Flow velocity	30	m/s
Magnetic field	0–20	T
Duct loading:	continuous electrode with insulating sidewalls	
• average electric load factor	0–20	
• load potential	0–6000	V

The physical properties of seawater are documented in Ref. 10; the values used are for a temperature of 20°C.

Parametric Study

A parametric study has been performed by varying the magnetic field up to 20 T, and the average electric load factor between 1 and 20. The average electric load factor K is defined as

$$K = \langle E_y \rangle / \langle uB \rangle$$

No restrictions have been imposed in this study on the flow conditions at the exit of the thruster. The computations proceed to compute the flowfields and the pressure increase along the thruster regardless of the actual ambient pressure. Practically, for steady-state conditions, the flow velocity inside the thruster is a floating parameter that will be determined by the input and boundary conditions of the propulsion system. The cruise velocity will be reached when there is balance between the total thrust generated and the total surface drag of the ship or submarine. Furthermore, we will limit the discussion to cases of high magnetic fields (20 T), where flow distortions are more likely to occur.

Effect of Load Factor on the Global Performance Parameters

Figure 2 presents the results for the pressure gain along the thruster for different load factors for the case of $B = 20$ T and flow velocity equals 30 m/s. Also presented on Fig. 2 is a curve for the accumulated frictional losses along the duct of the thruster. There is a linear dependence of the pressure gain on the axial distance along the duct. Such linear dependence is expected, since the physical properties and the average axial velocity are constants along the duct. For simple MHD flows with no Hall effect ($\beta = 0$), the pressure rise is given as

$$\Delta p = (J_y B)\, L = \sigma u B^2 (K - 1)\, L \qquad (14)$$

This simple relationship indicates that the pressure gain varies linearly with the distance x along the duct, and increases with the load factor. This does not suggest MHD thrusters should operate at higher values of the load factor, because this, as discussed later, leads to lower efficiencies.

Figure 3 demonstrates the variation of the electrical efficiency with the load factor for $B = 20$ T. Two curves are shown on this figure: the top curve is for the ideal electrical efficiency, and the bottom curve is the result of the three-

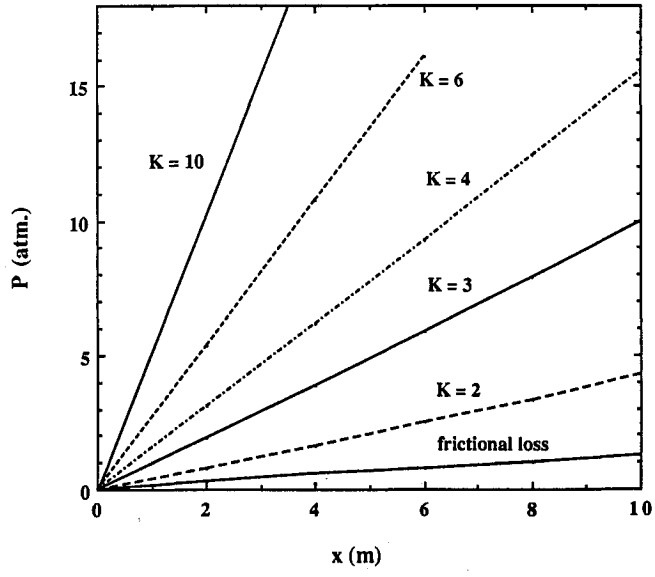

Fig. 2 Pressure rise along the thruster ($B = 20$ T, $U = 30$ m/s).

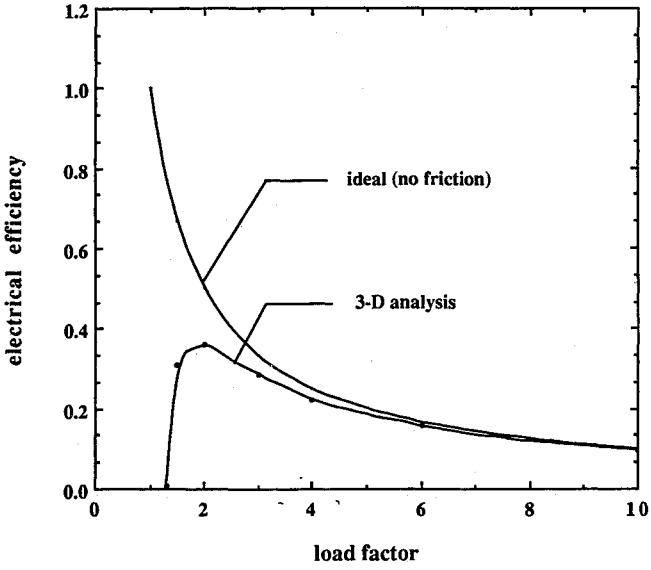

Fig. 3 Variation of the electrical efficiency with load factor (B = 20 T, U = 30 m/s).

dimensional calculations of the flowfields. In general, the thruster electrical efficiency is defined as

$$\eta_e = \frac{\Delta p Q}{VI} \tag{15}$$

where Δp is the pressure rise along the duct, Q is the volumetric flowrate, and V and I are the applied external voltage and currents. Physically, this efficiency represents the net resulting MHD push power (after subtracting the frictional losses) divided by the input power.

The electrical efficiency considered here does not include other losses, such as the end losses due to the fringing of the magnetic field near the ends of the electrode. The overall efficiency of the MHD thruster system includes other losses in the different components of the thruster system, such as the nozzle losses at the entrance of the thruster and the loss of kinetic energy at the exit of the jet. This is a subject of a different study discussed elsewhere by one of the authors.[11]

For ideal situations, where the flow is treated as one-dimensional with constant properties and neglecting all losses except Ohm's losses, one can show that the thrust efficiency is given by

$$\eta_{\text{ideal}} = uB/E_y = 1/K \tag{16}$$

This simple relationship is shown in Fig. 3, and it indicates, as expected, that the ideal efficiency is 100% for a load factor of 1 (open circuit). In this case, no thrust is being generated. If frictional losses are included in the analysis, the thruster efficiency decreases, as shown in the figure. However, since the frictional losses along the duct are almost the same for all values of K (as shown in Fig. 2), the deviation of the computed values of the thruster electrical efficiency from the ideal values gets larger as the load factor K decreases. As a matter of fact, the curve for the computed electrical efficiency eventually reaches a peak, and then changes its slope at lower values of K when the net pressure gradient (after subtracting the frictional losses) gets smaller and can become negative. This situation takes place when the MHD $J \times B$ forces become less than the frictional losses.

The maximum electrical efficiency of the thruster in this particular case is about 38%, and occurs at a load factor close to 2. This poor efficiency is attributed to the large frictional losses encountered for rough walls (2.5 mm) and for high flow velocities (30 m/s), and it is not in any way the optimum. For open-cycle MHD generators, such a value for the wall roughness is reasonable because of electrode segmentation, among other reasons. However, for MHD seawater thrusters, where continuous electrodes are expected to be used, the duct walls can be assumed to be practically smooth. The computations were repeated for this situation, and a maximum electrical efficiency of 59.2% was achieved at a load factor K = 1.4. Furthermore, when the flow velocity was reduced to a value of 10 m/s, a maximum electrical efficiency of about 74% was achieved, at a load factor K = 1.2.

This discussion suggests greater attention should be given to the calculation of the frictional losses at lower values of the load factor K, particularly for K between 1 and 2, because of its strong influence on the thruster efficiency. This issue is very important for the viability of MHD seawater propulsion, as has been discussed in more detail in Ref. 11.

Flowfields and Friction Factor

In order to predict the frictional losses accurately, one has to solve for the development of the flowfields inside the MHD thruster. Figure 4 illustrates the axial velocity profiles in the boundary layers over the electrode wall and the sidewall at the exit of the MHD duct. As shown in this figure, there is a difference between the shape of the axial velocity profile along the electrode and that along the sidewall (flatter over the sidewall). The velocities near the insulating sidewalls are relatively higher than those near the electrode walls. Clearly, this distortion is a result of the MHD forces (J_yB) acting in the momentum equations.

In order to understand this behavior further, it is necessary to consider the development of the J_y distribution between the two insulating sidewalls. The current distribution depends on several factors, mainly, the electrical connection, electrical conductivity distribution, and velocity field. In the present study, the thruster is connected in the Faraday mode with continuous electrodes and with electrically insulating sidewalls. Therefore, there is no flow of current through the sidewalls. If all properties and the flowfields were uniform, J_y would be uniform, and a uniform accelerating force would have been imposed on the flow. However, in our case, the velocity field is not uniform, whereas the conductivity is constant. For the present application, where the Hall parameter is zero, Ohms law gives the following:

$$J_y/\sigma = (E_y - uB) \tag{17}$$

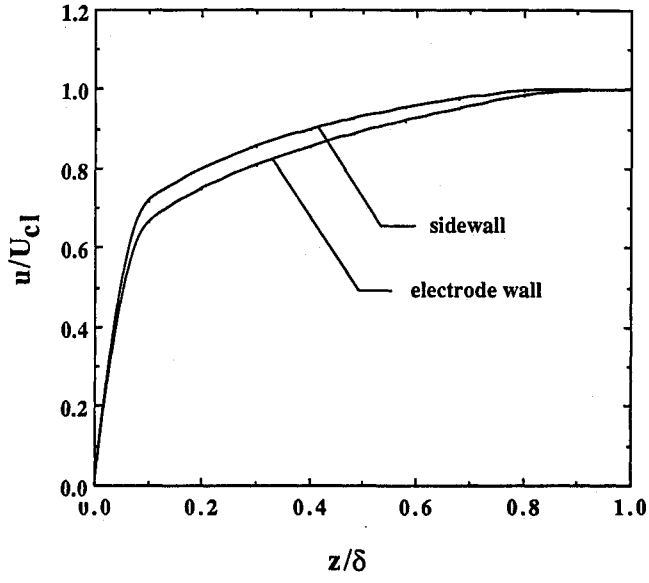

Fig. 4 Normalized velocity profiles along the thruster walls (B = 20 T, U = 30 m/s, x = 10 m).

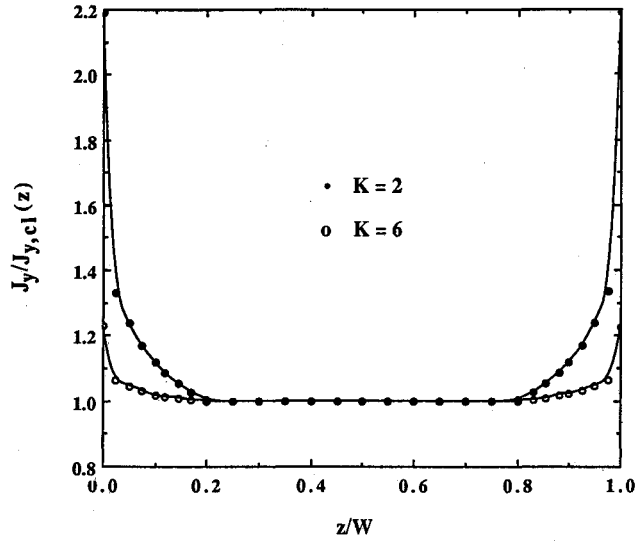

Fig. 5 Normalized current density across the sidewall for two load factors (B = 20 T, U = 30 m/s).

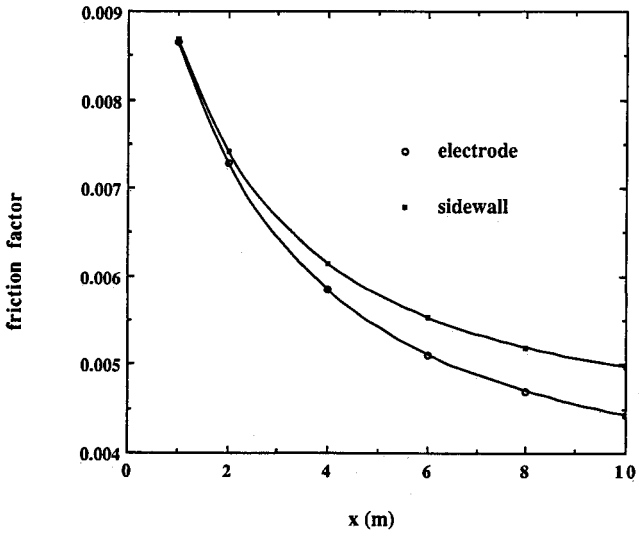

Fig. 6 Variation of the friction factor along the thruster walls (B = 20 T, U = 30 m/s).

Qualitatively, one can argue that $E_y(z)$ can be assumed constant for a Faraday connection with continuous electrodes, where

$$\int_o^H E_y(z)\,dy = \text{applied voltage} = \text{constant} \qquad (18)$$

where H is the height of the duct (distance between the electrodes). Consequently, J_y will be higher in magnitude near the sidewall than at the center of the flow. Furthermore, if the load factor for simplicity is defined as $K = E_y/(u_{cl}B)$, then

$$\frac{J_{y_z=0}}{J_{y_z=W/2}} = \frac{K}{(K-1)} \qquad (19)$$

For MHD thrusters, the load factor K is greater than one. Therefore, from the above relationship, J_y is expected to be higher near the sidewall than in the core of the flow, and their ratio is expected to increase for lower load factors.

Figure 5 shows the distribution of the J_y component of the current density (normalized to the centerline value) across the duct between the insulating walls at x = 10 m and, for load factors, K = 2 and 6. This distribution, along the boundary layers of the sidewalls (known as Hartmann layers), results in flow distortion. The nonuniform J_y distribution accelerates the flow differentially, exerting a larger force on the sidewall boundary layers, and leading to flatter boundary layer profiles in comparison to the electrode wall boundary layers. (Such behavior is depicted in Fig. 4, and is known as the Hartmann effect.) As a result of such nonuniformities in the flowfield, nonuniform distribution of the skin friction is expected along the duct walls. Figure 6 presents the variation of the friction factor (C_f) along the electrode wall and the sidewall of the thruster. The skin friction is higher on the sidewall because of the Hartmann effect.

The same mechanism responsible for the flattening of the boundary layers along the sidewalls and the increase of the skin friction factor for MHD thrusters is the cause for the velocity overshoots in MHD plasma generators, albeit for different reasons. In MHD generators, the boundary layers are colder, and this leads to lower electrical conductivity in the near-wall regions, which leads to lower absolute values of the current density J_y. However, the J_yB forces act to retard

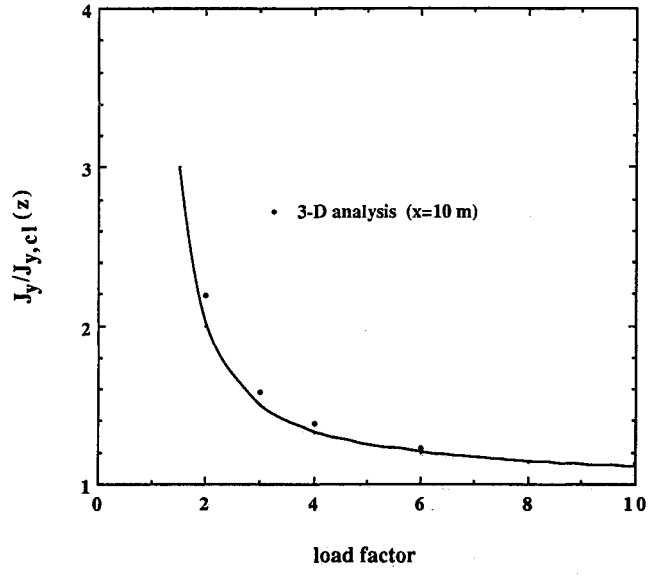

Fig. 7 Effect of load factor on the current density along the sidewall (B = 20 T, U = 30 m/s).

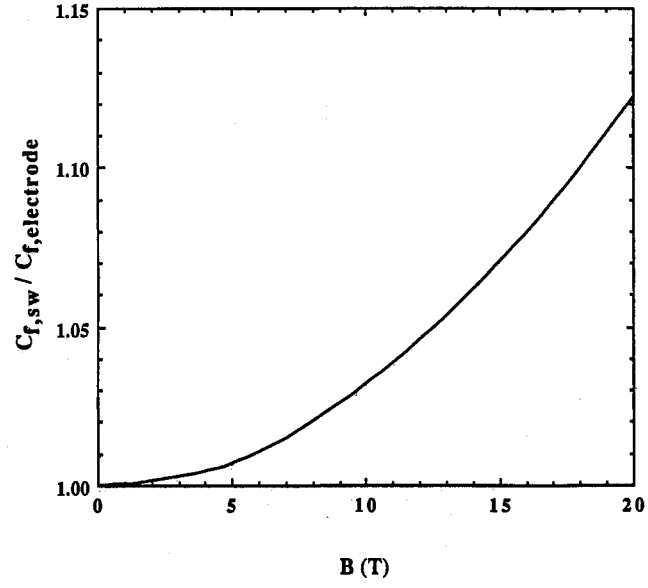

Fig. 8 Effect of magnetic field on the ratio of the friction factors along the thruster walls (U = 30 m/s, x = 10 m).

the flow in MHD generators. This results in a larger retarding force in the central region of the flow. In a relative sense, the sidewall boundary layers are accelerated in relation to the central region, and this leads to the known phenomenon of velocity overshoots. Such a phenomenon is discussed in more detail in Ref. 7.

Figure 7 illustrates the variation with the load factor K of the normalized current density $J_y(z)$ at the sidewall to the core value at the exit of the thruster for $B = 20$ T. The curve represents the previously given simple relationship [Eq. (19)] $K/(K - 1)$, whereas the points represent the results of the three-dimensional calculations.

Finally, Fig. 8 shows the effect of the magnetic field on the ratio of the skin friction between the sidewall and the electrode wall at the exit of the thruster ($x = 10$ m). As we might expect, the difference in the behavior between the electrode and sidewalls, in terms of the skin friction factor, increases as the magnetic field increases.

Summary and Conclusions

1) A three-dimensional MHD computer model has been developed and applied in the parametric study to investigate the concept of MHD seawater propulsion. A constant area duct with rectangular crossection has been used in the applications of MHD propulsion. The thruster is assumed to operate in the Faraday mode with continuous electrodes and insulating sidewalls and with an external applied voltage.

2) As the load factor decreases, the thruster efficiency increases. However, as the load factor keeps decreasing, a peak is reached in the thruster efficiency curve, and then the efficiency starts to decrease rapidly as the generated MHD $J \times B$ forces gets smaller in comparison to the frictional losses, which remain almost constant regardless of the load factor (for a constant flow velocity). Therefore, greater attention should be given to the calculation of the frictional losses at lower values of the load factor K, particularly for load factors between 1 and 2. Frictional losses should be minimized in order to achieve higher thruster efficiencies.

3) The Hartmann layers on the insulating sidewalls are shown to have important effects on the current density and velocity distributions in the sidewall boundary layers. The velocity profiles are flatter over the sidewalls in comparison to the velocity profiles over the electrode walls. As a result, the average skin friction factor is enhanced along the sidewalls, in comparison with the skin friction factor along the electrode wall.

Assuming that one can achieve reasonably high values of thruster efficiencies, there still remain several important technical issues that can be potential show stoppers for the application of this propulsion concept. Among these issues are the construction of practical high-strength superconducting magnets and their support structure of reasonable mass, and the elimination of the magnetic signatures to acceptable levels within and away from the ship or submersible. Another issue is the production of bubbles from seawater due to electrolysis and their impact on electrode material, acoustic signature, and thruster performance. All these issues and others are important and should be addressed; however, they are beyond the scope of this paper.

Acknowledgment

This work has been sponsored by the U.S. Office of Naval Research, under Contract No. N00014-89-F-0064.

References

[1]Phillips, O. M., "The Prospects for Magnetohydrodynamic Ship Propulsion," *Journal of Ship Research*, Vol. 43, March 1962, pp. 43–51.

[2]Doragh, R. A., "Magnetohydrodynamic Ship Propulsion Using Superconducting Magnets," *Society of Naval Architects and Marine Engineers, SNAME Transaction*, Vol. 71, 1963, pp. 370–386.

[3]Way, S., "Electromagnetic Propulsion for Cargo Submarines," *Journal of Hydraulics*, Vol. 2, No. 2, 1968, pp. 49–57.

[4]Saji, Y., Kitano, M., and Iwata, A., "Basic Study of Superconducting Electromagnetic Thrust Device for Propulsion in Seawater," *Advances in Cryogenic Engineering*, edited by K. D. Timmerhans, Vol. 23, 1978, pp. 159–169.

[5]Hummert, G. T., "An Evaluation of Direct Current Electromagnetic Propulsion In Seawater," Report ONR-CR168-007-1, Westinghouse Research Lab., Pittsburgh, PA, July 1979.

[6]Cott, D. W., Daniel, V. W., Carrington, R. A., and Herring, J. S., "MHD Propulsion For Submarines," CDIF External Report No. 2, DOE-MHD-D140, MSE Inc., Butte, MT, Oct. 1988.

[7]Doss, E. D., and Curry, B. P., "Studies of the 3-D Coupled Flows Between the Electrode and Sidewalls of MHD Channels," AIAA Paper 76-311, AIAA 9th Fluid and Plasma Dynamics Conference, San Diego, CA, July 1976.

[8]Doss, E. D., and Ahluwalia, R. K., "Three-Dimensional Flow Development in MHD Generators at Part Load," Journal of Energy, Vol. 7, No. 4, July–August 1983, pp. 289–290. Also AIAA Paper No. 82-324, AIAA 20th Aerospace Sciences Meeting, Orlando, Florida, Jan. 1982.

[9]Vanka, S. P., Ahluwalia, R. K., and Doss, E. D., "Three-Dimensional Analysis of MHD Generators and Diffusers," Report No. ANL/MHD-82-4, Argonne National Laboratory, Argonne, Illinois, March 1982.

[10]*McGraw-Hill Encyclopedia of Science and Technology*, 6th Ed., Vol. 16, McGraw-Hill, NY, 1987, pp. 144–178.

[11]Doss, E. D., and Geyer, H. K., "Effects of Friction and End Losses on MHD Thruster Efficiency," *Proceedings of the 28th Engineering Aspects of Magnetohydrodynamics*, Chicago, IL, June 26–28, 1990, pp. III.2-1–III.2.8.